Experimental analysis of self-organized structure and transport on the magnetospheric plasma device RT-1

journal or publication title	Nuclar Fusion
volume	59
number	9
page range	096005
year	2019-07-17
URL	http://hdl.handle.net/10655/00012778

doi: 10.1088/1741-4326/ab259a

Creative Commons : 表示 - 非営利 - 改変禁止
http://creativecommons.org/licenses/by-nc-nd/3.0/deed.ja

Experimental analysis of self-organized structure and transport on magnetospheric plasma device RT-1

M. Nishiura[1,2], Z. Yoshida[2], N. Kenmochi[2], T. Sugata[2], K. Nakamura[2], T. Mori[2], S. Katsura[2], K. Shirahata[2], J. Howard[3]

[1]National Institute for Fusion Science, Gifu 509-5292, Japan

[2]Graduate School of Frontier Sciences, The University of Tokyo, Chiba 277-8561, Japan

[3]Plasma Research Laboratory, Australian National University, Canberra, Australia

E-mail contact of main author: nishiura@nifs.ac.jp

Abstract.

The dipole plasma exhibits strong heterogeneities in field strength, density, temperature, and other parameters, while maintaining the holistic balance. Enquiring into the internal structures, we reveal the fundamental self-organizing mechanisms operating in their simplest realization (as commonly observed in astronomical systems). Three new findings are reported from the RT-1 experiment: Creation of a high-energy electron core (similar to the radiation belts in planetary magnetospheres) is observed for the first time in a laboratory system. High-energy electrons (3 – 15 keV), produced by an electron cyclotron heating (ECH), accumulate in a "belt" located in the low-density region (high-beta value ~ 1 is obtained by increasing the high-energy component up to 70% of the total electrons). The dynamical process of the "up-hill diffusion" (a spontaneous mechanism of creating density gradient) has been analyzed by perturbing the density by gas injection. The spontaneous density formation in laboratory

magnetosphere eluciates the self-organized plasma transport relevant to planetary magnetosphere. The coherence-imaging spectroscopy visualized the two dimensional profiles of ion temperature and flow velocity in the ion cyclotron resonance frequency (ICRF) heating. The ion temperature and flow were enhanced globally, and particularly along the magnetic field lines near the levitation magnet. These results advance our understanding of transport and self-organization not only in dipole plasmas, but also in general magnetic confinement systems relevant to fusion plasmas.

1. Introduction

Plasma confinement in a dipole magnetic field is studied for advanced nuclear fusion, which is motivated from the natural formation on high beta plasmas in a planetary magnetosphere. The strong inhomogeneity of the dipole magnetic field is the root cause of various interesting phenomena. The self-organization of plasmas is an inherent mechanism, and manifests as holistic phenomena creating and sustaining this localized structure [1, 2]. The particle transport characterizes a turbulent diffusion driven by the electric-field fluctuations observed in a laboratory magnetospheric plasma of the LDX [3]. The common transport principle dominates in a laboratory and a planetary magnetospheric plasma. The satellite measurements observed high energy particles and stable high beta plasmas in planetary magnetospheres [4].

The original work of a dipole device was conducted by S. Yoshikawa as the Princeton spherator and reviewed in 1973 [5] to answer a magnetically confined fusion reactor in view of anomalous transport, turbulence, and instability. He also considered the spherator as a particle trap for non-neutral plasma research. The plasmas in spherators are confined in between the center stack and the internal magnet. The main confinement area is different from

a dipole device considered in this paper. The timeline of dipole devices for plasma physics and dipole fusion start from the proto-RT with an internal-normal conductor which is fixed by support rods. The Mini-RT with a compact levitation ring magnet operated from 2003 to 2018. The recent study was focused on the excitation of electron Bernstein wave to produce a high-density plasma in low magnetic fields [6]. The Ring Trap 1 (RT-1) device experiments subsequently started in 2006 [7, 8]. The experiments for dipole plasma confinement also started at the LDX [9] in this stage. An internal-levitation superconducting-ring magnet in the RT-1 produces a dipole field such as a laboratory magnetosphere (see Fig. 1). Only the poloidal field exists for the dipole plasma confinement. The ring structure of a levitation magnet is designed to reduce the end loss of particles, and therefore the passing particles are well confined in a dipole field. The dipole confinement is considered to become an advanced fusion machine with the suppression of loss cone particles in a linear machine as well as the field ripple effect in tokamak and helical devices.

The performance of the RT-1 was reported in the ref. [10]. To obtain the empirical formula of the beta value from the measured diamagnetic signal in the RT-1, the plasma equilibrium was analyzed by combining a magnetic field measurement and the solution of the Grad-Shafranov equation. The RT-1 device realized stable confinement of high-beta plasma (local electron beta > 1) by the electron cyclotron (EC) heating. From the x-ray measurement, it was found that the high energy electrons in the range of a few ten keV sustain the high beta plasmas. The electrons with the energies of a few ten eV and keV concomitantly existed in high beta plasmas of the RT-1.

The perpendicular and parallel ion temperatures were typically $T_{\perp} \sim 30$ eV and $T_{\parallel} \sim 10$ eV, respectively. The cold electron temperature T_{ec} was around 60 eV from the line integrated helium line spectroscopy. In this operation range, examining the energy balance model, the spontaneous heating power due to the betatron effect was separated from the auxiliary heating

[11]. The beta value in the RT-1 is mainly dominated by high energy electrons. The increase in ion beta against the total beta was desired from the viewpoint of ion confinement and fusion machine. However, the ion temperature was still in the range of ~ 50 eV. For the ion heating, the ICRF heating system has been designed and developed in the RT-1 [12, 13]. The beach heating scheme [14] is usually applied to the linear machine. The scheme was demonstrated firstly in a magnetospheric plasma where the field gradient and direction is different. The slow wave was excited by a double-loop antenna at the inner high field side (B ~ 0.52 T) in the inhomogeneous field near the pole area. The slow wave propagates along the magnetic field toward the ion cyclotron resonance layer (B ~ 0.13 T). The effect of the ICRF heating has a spatial distribution, and the effect was particularly significant for ion temperature and flow in the core region from the spectroscopic measurement. The profile of electron density was modified by the ICRF heating.

To understand the transport of self-organized plasmas and the heating effect in magnetospheric plasmas, a Thomson scattering (TS) for the electron temperature and density [15], and the coherence imaging spectroscopy (CIS) [16] have recently been implemented in the RT-1 [17]. The existing diagnostics can explain the local and entire plasma dynamics.

2. HIGH ENERGY ELECTRON CORE IN DIPOLE CONFINEMENT SYSTEM

The operation regimes of the electron density and the beta value in the RT-1 have been reported [10]. The internal structure of high-energy electron-component is investigated in a plasma with a moderate beta (~ 0.2). The line-integrated x-ray emissions of 3 vertical chords (SD1 at r = 0.60 m, SD2 at r = 0.72 m, and SD3 at r = 0.84 m) and one horizontal chord (SD4 scannable in horizontal direction) are measured by Si detectors. A pin hole made of lead is equipped in front of each detector. The thickness of the pin hole is optimized to prevent stray

noise from the plasmas. The line-of-sight is scanned horizontally shot by shot. These line-integrated data are reconstructed to obtain the spatial profile of the high energy electron component. The model functions for high energy electron density n_{model} (r, z) and temperature T_{model} (r, z) are given as a function of the magnetic flux surface $\psi(r, z)$, and are given by

$$n_{\mathrm{model}}(r,z) = n_0 \exp\left(-a\left(\frac{\psi(r,z)-\psi(r_{\mathrm{max}},0)}{\psi(1,0)}\right)^2\right)\left(\frac{B(r,z)}{B_0(r,z)}\right)^{-b} \qquad (1)$$

$$T_{\mathrm{model}}(r,z) = T_0 \exp\left(-a'^{\left(\frac{\psi(r,z)-\psi(r_{\mathrm{max}},0)}{\psi(1,0)}\right)^2}\right) \qquad (2)$$

Here, the parameters a, b, and a' are determined by fitting the measured data. The term $\left(\frac{B(r,z)}{B_0(r,z)}\right)^{-b}$ appears in this model to express the trapped orbits of the particles in a poloidal plane. Considering the solid angle $\Delta\Omega(r, z)$ at a detector and the volume $\Delta V(r, z)$, where the photon emission occurs, the photon number $N_{\mathrm{model}}(r, z)$ to be measured in the detector is

$$N_{\mathrm{model}}(r,z) = n_{\mathrm{model}}(r,z)\, n_{ion}(r,z)\, Z_{\mathrm{eff}}^2 \frac{\exp\left(-\frac{E_j}{T_{\mathrm{model}}(r,z)}\right)}{E_j\sqrt{T_{\mathrm{model}}(r,z)}}\Delta\Omega(r,z)\Delta V(r,z) \qquad (3)$$

It is assumed that the effective charge $Z_{\mathrm{eff}} \sim 1$, and n_{ion} (r, z) $\sim n_{\mathrm{e}}$ (r, z). The reconstructed profiles for the total electrons and the high energy component are shown in FIG. 2. The x-ray spectrum in the range of 3–15 keV is used for the reconstruction of high-energy electrons. The high-energy electrons form the toroidal "belt" structure in the outer low-density region. We found the creation of strongly localized "belt" structure in the plasma, and the cold electrons exist concomitantly. The local electron beta is estimated to be about 0.3 from a kinetic temperature of high-energy electrons. This beta value is consistent with that estimated from the diamagnetic signals. From the x-ray measurement, the local beta is proportional to the line averaged density of high energy electrons at the edge sightline, but not at the core sightline. The experimental results suggest the "belt" structure at the edge region such as a radiation belt in magnetosphere. In the highly collisionless plasmas, electrons have strongly

non-equilibrium and anisotropic velocity distribution. It is considered that the situation makes it possible for the high-energy (> 10 keV) and low-energy (< 0.1 keV) components to coexist in plasmas. The high-energy component contributes to the high beta, in which the high-energy component is dominant (~ 70 %). The rate equations in RT-1 plasmas explain the coexistence of high and low energy components. The high energy electrons are populated near the plasma edge (FIG. 2 (b)). When the electron density exceeds above the cut off density as shown in FIG. 2 (a), the EC wave launched from the equatorial port cannot reach the fundamental ECR layer directly. In this situation, the high-energy electrons are populated as trapped orbits, because the wave might be absorbed around $(r, z) = (0.3, \pm 0.2)$.

In view of the EC heating in inhomogeneous field, the propagation and the heating efficiency of the EC wave are simulated by using the 2D full wave code. The cold plasma dielectric tensor is used to calculate the wave propagation in plasmas. The EC wave with 2.45 GHz is injected from the equatorial plane at $(r, z) = (1.0, 0)$. At the initial stage of the discharge, the EC heating starts up the discharge on the fundamental resonance layer at $(r, z) = (0.4, 0)$, and sustains the plasma. The electron density in front of the resonance layer grows to the cut off density. The cut off layer for the O mode reflects the wave toward the vessel. Finally, the multi-reflected waves reach some areas of the EC resonance (ECR) layer from high field side. This is one of the scenarios for continuous EC heating.

As another possible heating scenario, the mode conversion to electron Bernstein wave can access to the high density region beyond the cut off density. Although the possibility has been studied in the mini-RT [6], further studies are required to explain the over dense results of the RT-1.

From the experimental results, we found that the reconstructed profile of the electron density at the maximum exceeds the cut off density. Because the density peak is not located

on the ECR layer, the up-hill diffusion would drive the particle transport as the theory predicts [2]. Similar results have been reported in the LDX [3].

3. SELF-ORGANIZED PLASMA AND UP-HILL DIFFUSION

A peaked density profile is spontaneously produced through the up-hill diffusion [2, 10], where the particles diffuse toward higher density area. In the previous section, we described the transport from the viewpoint of wave heating. The particle transport on up-hill diffusion is demonstrated experimentally by injecting tracer gas into helium plasmas. Figure 3 shows the time evolution of the line-integrated densities measured by interferometers. At t = 1.1 s, the helium gas is puffed for 5 ms into the helium plasma. The line-integrated density of the horizontal chord at r = 0.45 m increases rapidly by about 10%, and starts decreasing at t = 1.38 s. The densities of other two chords decrease just after the gas puffing. The difference of reconstructed electron density profiles between t = 1.38 s and 1.12 s is plotted in FIG. 4. The spontaneous increase in the electron density appears clearly at r = 0.55 m. The area differs from the fundamental and the second harmonic ECR layers, where the plasma is produced. From the particle balance equation, He^+ is ionized within ~ 10 ms, and the electron density increases rapidly within 20 ms. The neutrals are supplied from the wall by the recycling particles uniformly. Therefore, the spontaneous modification of the density profile would be due to the up-hill diffusion. This feature supports the fact that the heating beams with 2.45 GHz and 8.2 GHz produce the densities higher than the cut off densities. The density fluctuation with ~ 0.6 kHz was observed by the outer interferometers simultaneously in this period. This is the order of the drift frequency in the toroidal direction. Our result supports the observation of turbulent particle transport toward higher magnetic fields reported by Boxer et al. [3]. However, the relation between the observed coherent mode with ~ 0.6 kHz and the transport needs to be studied.

4. 4. ICRF HEATING AND ITS EFFECT IN DIPOLE CONFINEMENT

The spontaneous toroidal ion flow is observed in the RT-1 plasmas. Theoretical work expects that this ion flow improves the plasma confinement [18]. The observed toroidal flow velocity is expressed as the sum of drift velocities,

$$V_{obs} = \frac{m{v_\parallel}^2}{R^2}\frac{\boldsymbol{R}\times\boldsymbol{B}}{qB^2} - \frac{m{v_\perp}^2}{2}\frac{\boldsymbol{B}\times\nabla\boldsymbol{B}}{qB^3} - \frac{\nabla(nkT_i)\times\boldsymbol{B}}{qnB} + \frac{\boldsymbol{E}_\perp\times\boldsymbol{B}}{qB^2} \ . \qquad (4)$$

The ion flow velocity on the equatorial plane was measured by a grating spectrometer. The result shows that the $\boldsymbol{E}\times\boldsymbol{B}$ drift dominates the toroidal flow in the core region. In homogeneous fields, these terms change spatially.

The ion cyclotron resonance of frequency (ICRF) heating was successfully demonstrated in magnetospheric plasmas [13]. The slow wave was excited by a double loop antenna in the high field side near the center stack as is shown in FIG. 5. The ion temperature was increased in the confinement region, while the ion flow is enhanced near the levitation magnet [12]. Coherence imaging spectroscopy (CIS) [17] was newly implemented to understand the heating mechanism and its effect on a poloidal cross section. In helium plasmas, the CIS measured the spectral intensity, the ion temperature, and the flow velocity of He^+ in FIG. 6. The input powers of 10 kW for the ECH sustained the target plasma. Just after 0.1 s from the ECH injection, the ICRF heating of 9.4 kW was applied to the double loop antenna up to the termination of the discharge. The CIS was measured for the exposure time of 0.8 s in the stable density period. The ICRF heating increased the He^+ intensity globally in the plasma confinement region, particularly along the magnetic field lines near the levitation magnet. The ion temperature of He^+ also had the same profile. The ion flow was accelerated near the levitation magnet. These parameters are effectively enhanced at the locations where the He^+ emission is intense in the EC heating. The low He^+ emission region is appeared around the

maximum electron density (see FIG. 2 (a)). Suppose $n_e \sim n_i$, the He^{2+} ions would be dominant in the good confinement region. For the detailed discussion, we should obtain the local ion flow in a poloidal cross section from the line-integrated flow. The reconstruction by the velocity tomography method [19] is under the way because of the accuracy in the case including the low intensity region.

5. Summary

The results are summarized as follows: (i) The population of the high-energy electrons (which contribute to the high beta) have strongly heterogeneous profile. These high-energy electrons tend to localize in an outer low-density region and create a belt structure. (ii) The strongly peaked density profile is self-organized by the up-hill diffusion. By actively modifying the density profile with the gas injection, the dynamical process of up-hill diffusion, driven by density fluctuations in the drift-frequency regime of ~ 0.6 kHz, has been elucidated. (iii) The CIS diagnostic visualized the effect of the ICRF heating. The ion temperature and flow were enhanced globally, and particularly along the magnetic field lines near the levitation magnet.

Acknowledgments

This work was supported by the NIFS Collaboration research program (NIFS15KOAH034), and JSPS KAKENHI Grant No 17H01177.

References

[1] Hasegawa A., Comments Plasma Phys. Contr. Fusion 1 (1987) 147.

[2] Yoshida Z., Adv. Phys. X 1 (2016) 2.

[3] Boxer A. C., Bergmann R., Ellsworth J. L., Garnier D. T., Kesner J., Mauel M. E., Woskov P., Nature Phys. **6** (2010) 207.

[4] Persoon A. M., Gurnett D. A., Leisner J. S., Kurth W. S., Groene J. B., Faden J. B., J. Geophys. Res.: Space Phys. 118 (2013).

[5] Yoshikawa S., Nucl. Fusion **13** (1973) 433.

[6] Uchijima K., Takemoto T., Morikawa J., Ogawa Y., Plasma Phys. Control. Fusion. **57** (2015) 065003.

[7] Yoshida Z., Ogawa Y., Morikawa J., Watanabe S., Yano Y., Mizumaki S., Tosaka T., Ohtani Y., Hayakawa A., Shibui M., Plasma Fusion Res. **1** (2006) 008.

[8] Ogawa Y., Yoshida Z., Morikawa J., Saito H., Watanabe S., Yano Y., Mizumaki S., Tosaka T., Plasma Fusion Res. **4** (2009) 020.

[9] Garnier D. T., Hansen A., Mauel M. E., Ortiz E., Boxer A. C., Ellsworth J., Karim I., Kesner J., Mahar S., Roach A., Phys. Plasmas **13** (2006) 056111.

[10] Nishiura M., Yoshida Z., Saitoh H., Yano Y., Kawazura Y., Nogami T., Yamasaki M., Mushiake T., Kashyap A., Nucl. Fusion **55** (2015) 053019.

[11] Kawazura Y., Yoshida Z., Nishiura M., Saitoh H., Yano Y., Nogami T., Phys. Plasmas **22** (2015) 112503.

[12] Nishiura M., Kawazura Y., Yoshida Z., Kenmochi N., Yano Y., Saitoh H., Yamasaki M., Mushiake T., Kashyap A., Takahashi N., Nakatsuka M., Fukuyama A., Nucl. Fusion **57** (2017) 086038.

[13] Nishiura M., Yoshida Z., Yano Y., Kawazura Y., Mushiake T., Saitoh H., Yamasaki M., Kashyap A., Takahashi N., Nakatsuka M., Takase Y., Fukuyama A., Plasma and Fusion Res. **11** (2016) 2402054.

[14] Stix T.H. 1992 Waves in Plasmas(New York: American Institute of Physics) pp342-3.

[15] Kenmochi N., Nishiura M., Yoshida Z., Yamada I., Funaba H., Sugata T., Nakamura K., Katsura S., Rev. Sci. Instruments **89** (2018) 10C101.

[16] Howard, J., Michael C., Chen H., Lester R., Thorman A., Chung J., JINST **10** (2015) P09023.

[17] Nakamura K., Nishiura M., Takahashi N., Yoshida Z., Kenmochi N., Sugata T., Katsura S., Howard J., Rev. Sci. Instruments **89** (2018) 10D133.

[18] Yoshida Z., Mahajan S. M., Mizushima T., Yano Y., Saitoh H., Morikawa J., Phys. Plasmas **17** (2010) 112507.

[19] Howard, J., Plasma Phys. Control. Fusion **38** (1996) 489.

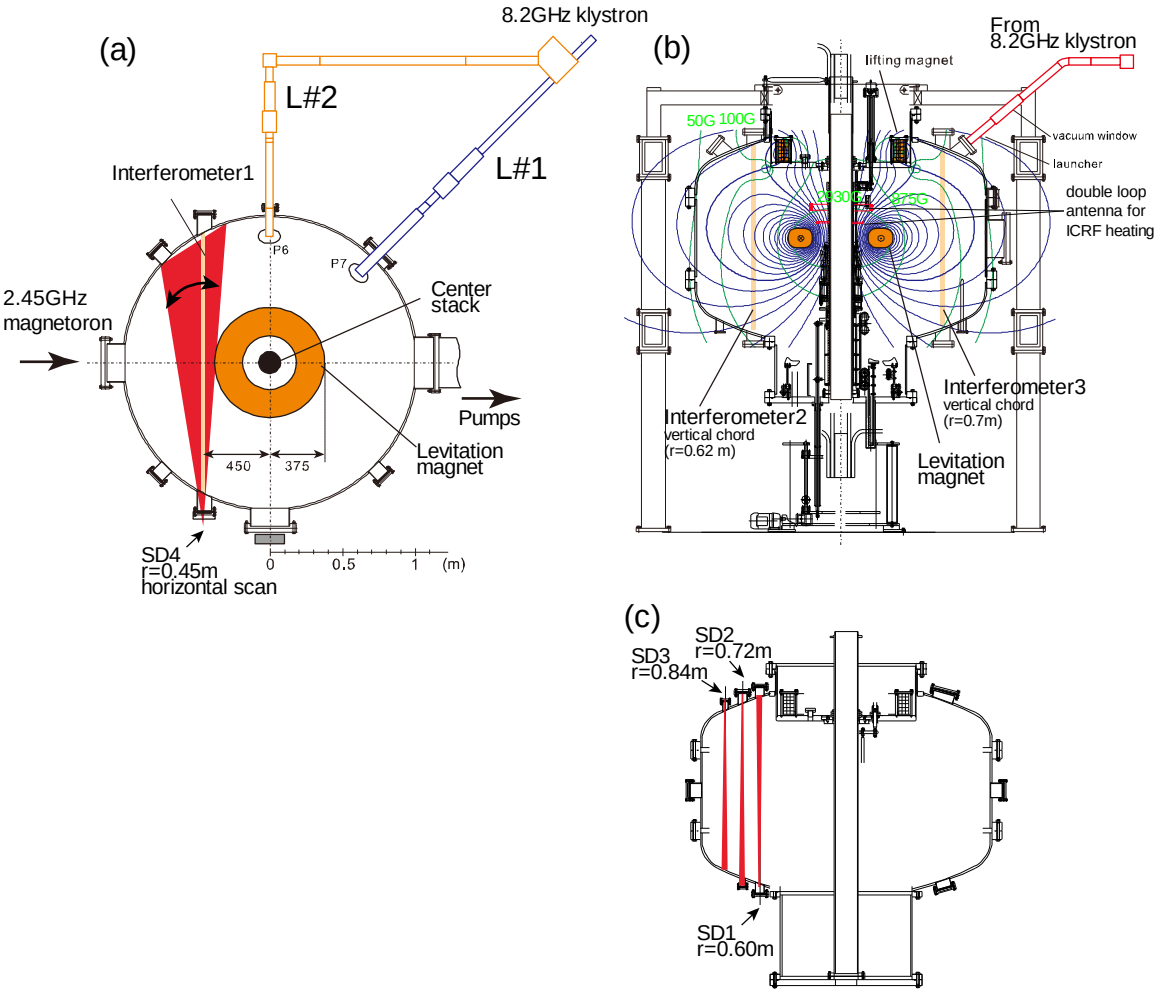

Fig. 1. (a) Midplane from the top. (b) and (c) cross sectional views of RT-1. The line of sights for interferometers are indicated. SD1, SD2, and SD3 indicate the vertical chords for x-ray detectors. SD4 scans horizontally on the midplane.

(a) (b)

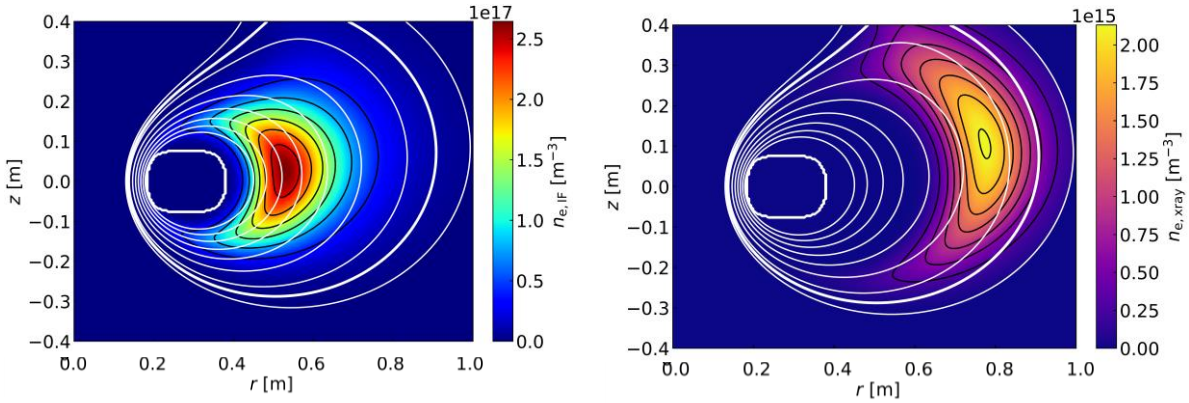

Fig. 2. Measured profiles of (a) the electron density and (b) the high-energy electrons. The spontaneous belt structure of high energy electrons is observed in outer radial location.

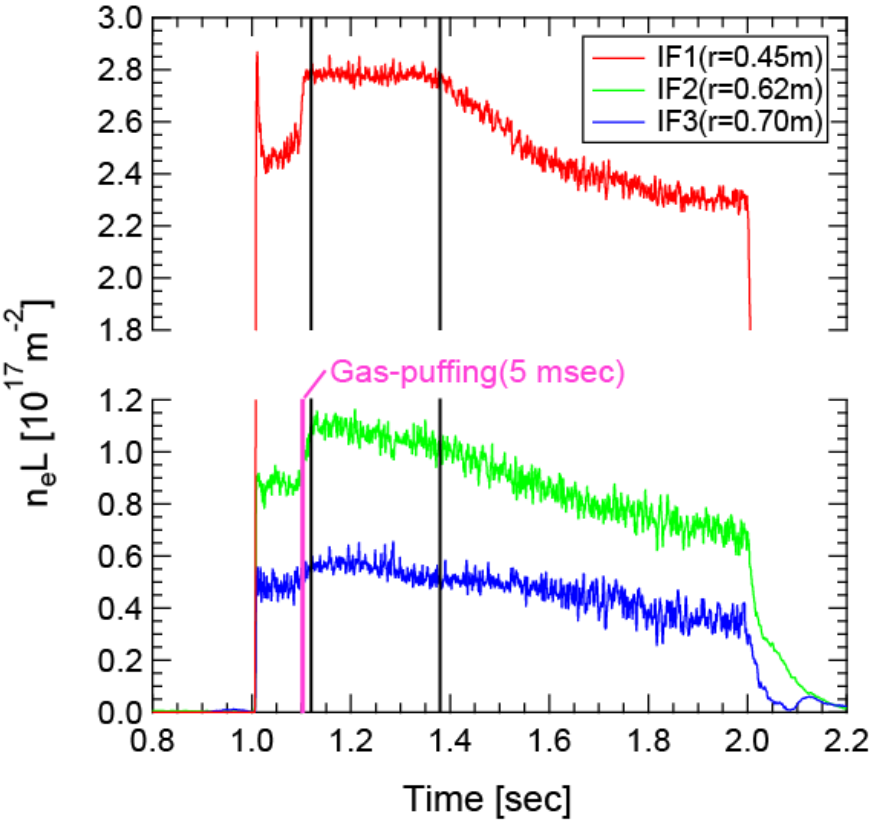

FIG. 3. Time evolution of the line-integrated densities where the chords of the interferometers pass through the inner and the outer edge regions (r = 0.45, 0.62, and 0.7 m are the innermost radii of the chords). The innermost chord IF1 observed the constant electron density from t = 1.12 to 1.38 sec (black lines), while the other chords decrease.

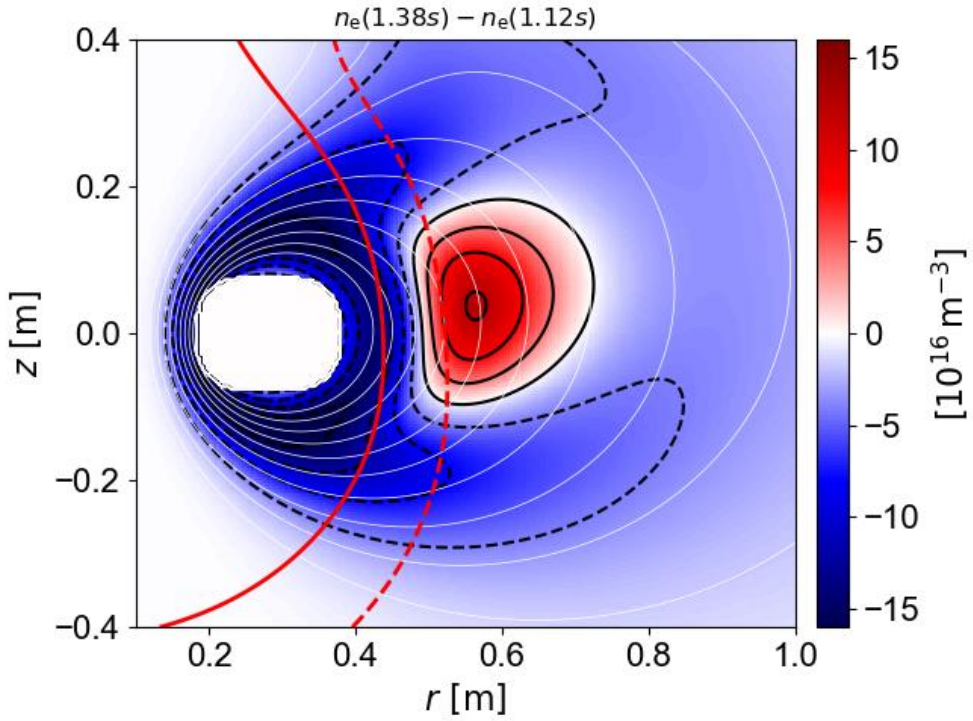

FIG. 4. Difference of the electron density. The reconstructed density profile at t = 1.38 s is subtracted from that at t = 1.12 s. The increase in the density is observed at r = 0.55 m. The locations for the fundamental and the second harmonic resonances are indicated by the solid and the broken curves in red.

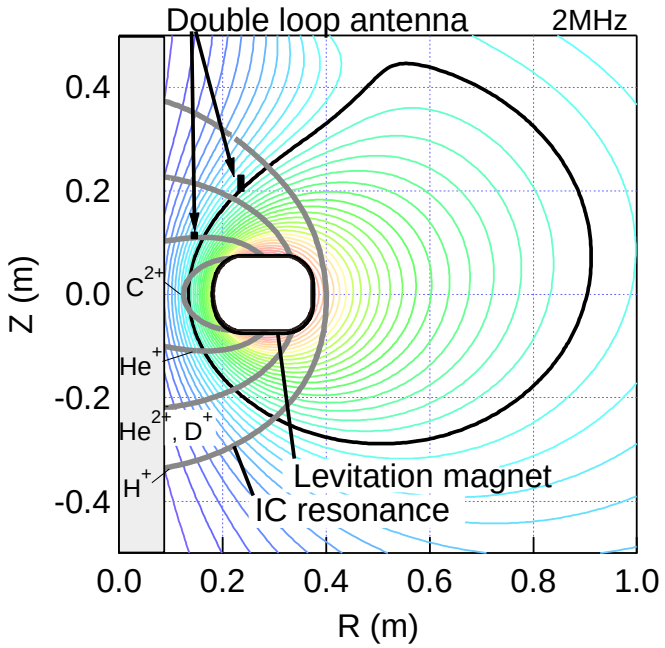

FIG. 5. ICRF antenna and ion cyclotron resonance layer in the RT-1.

(a) ICRF OFF

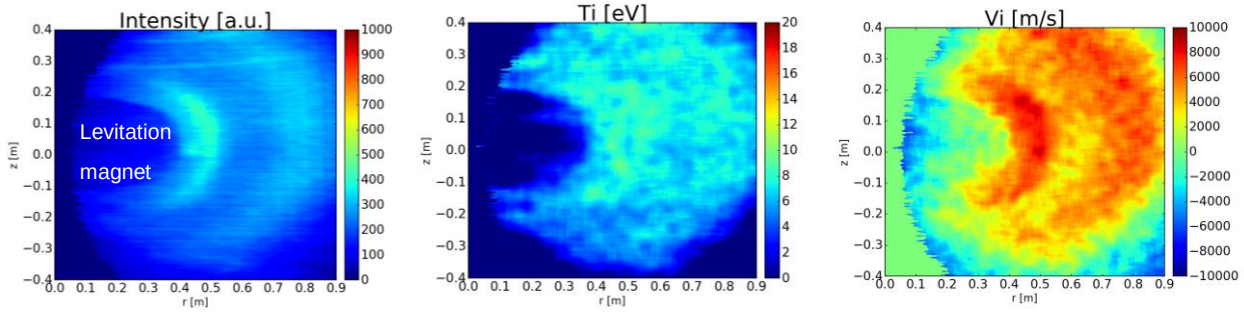

(b) ICRF ON

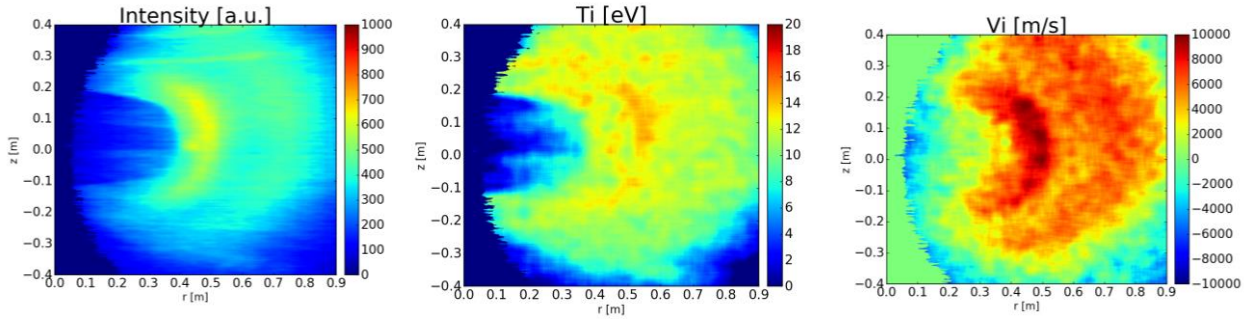

FIG. 6. Line-integrated emission intensity, temperature, and flow velocity of He^{+} in the case of ICRF off (upper row) and on (lower row). The ICRF heating increases the He^{+} intensity and the ion temperature.